Nuclear magnetic resonance restricted diffusion between parallel planes in a cosine magnetic field: An exactly solvable model

Denis S. Grebenkov[a)]
Laboratoire de Physique de la Matière Condensée, C.N.R.S.—Ecole Polytechnique, 91128 Palaiseau, France

(Received 5 October 2006; accepted 16 January 2007; published online 14 March 2007)

We propose a theoretical and numerical analysis of restricted diffusion between parallel planes in a cosine magnetic field. The specific choice of this spatial profile as proportional to an eigenfunction of the Laplace operator in this confining geometry considerably simplifies the underlying mathematics. In particular, exact and explicit relations for several moments of the total phase accumulated by diffusing spins are derived. These relations are shown to provide good approximations for the typical case of a linear magnetic field gradient, for which the theoretical analysis was in general limited to the second moment. We study the structure and the properties of the higher order moments which are responsible for the breakdown of the "Gaussian phase approximation" (GPA) at intense magnetic fields. The limits of applicability of the GPA for nonlinear magnetic fields and the transition to the localization regime are discussed. In particular, a diagram of different restricted diffusion regimes is presented. © *2007 American Institute of Physics*. [DOI: 10.1063/1.2539073]

I. INTRODUCTION

Nuclear magnetic resonance (NMR) monitoring of diffusing spins is a powerful experimental tool to investigate complex transport processes and to probe the geometry of confining porous media.[1–15] The macroscopic spin-echo signal produced by numerous nuclei moving in an inhomogeneous magnetic field may provide useful information about restricting boundaries. For a long time, the main attention was focused on the apparent diffusion coefficient (ADC) showing how the Brownian dynamics of spins effectively "slows down" with geometrical confinement. This characteristic of porous media was widely used in different applications, from oil recovery to medical diagnosis. For instance, ADC was shown to be related to the surface-to-volume ratio in rocks,[16–18] while ADC maps of human lungs might help to diagnose partial destruction of the alveolar tissue by emphysema.[19,20]

The notion of ADC is closely related to the Gaussian phase approximation (GPA) for the accumulated phase φ of spins diffusing in an inhomogeneous magnetic field. When this random variable follows a Gaussian distribution, the macroscopic spin-echo signal E is completely determined by its second moment $\mathbb{E}\{\varphi^2/2\}$,

$$E \propto \exp(-\mathbb{E}\{\varphi^2/2\}). \tag{1}$$

Hahn demonstrated this behavior for unrestricted (or free) diffusion in a linear magnetic field gradient.[21,22] In particular, the calculation of the second moment for a steady (bipolar) gradient of intensity g and duration T led to

$$E \propto \exp(-D\gamma^2 g^2 T^3/12), \tag{2}$$

where D was the (free) diffusion coefficient, and γ the gyromagnetic nuclear ratio. Since Woessner's experiments,[23,24] the Gaussian-type g^2-dependence in Eq. (2) was extended to restricted diffusion by replacing D by ADC.

A number of theoretical and numerical works dealt with the second moment of the accumulated phase. Stejskal and Tanner generalized the relation (2) to arbitrary temporal profile of a linear magnetic field gradient.[25] Robertson showed how the confinement between parallel planes at distance L could alter diffusive motion of spins at long times, yielding

$$E \propto \exp(-\gamma^2 g^2 T L^4/(120D)), \tag{3}$$

in the so-called motional narrowing regime.[26] Neuman used the Laplace operator eigenfunctions to extend these results to cylindrical and spherical confinements.[27] Stepisnik developed the density matrix calculation for a more general case including, for instance, strong dipolar coupling.[28,29] In particular, he related the NMR spin-echo attenuation in the magnetic field gradient to the velocity autocorrelation function. Tarczon and Halperin applied Fourier analysis to obtain the second moment in the case of a slab geometry and arbitrary spatial profile of the magnetic field.[30] Mitra *et al.* studied the second moment in the slow diffusion (or short-time) regime.[3,16,17] An overview of the above classical results can be found in Refs. 14 and 15.

Surprisingly, there is no evident mathematical reason for the Gaussian-type dependence (2) to hold for restricted diffusion in general. A pulsed-gradient spin-echo (PGSE) experiment[31] helps to illustrate this point. In contrast with Hahn's experiment, two very narrow gradient pulses (of duration δ) are applied to encode the positions of spins at times $t=0$ and $t=T$, resulting in signal proportional to the intermediate scattering function

[a)]Electronic mail: denis.grebenkov@polytechnique.edu

$$E \propto < e^{i\gamma\delta\mathbf{g}\cdot\mathbf{r}(0)} e^{-i\gamma\delta\mathbf{g}\cdot\mathbf{r}(T)} > , \quad (4)$$

with the average $<\ldots>$ over the whole ensemble of diffusing spins. If the diffusion time T between pulses is long enough, the positions $\mathbf{r}(0)$ and $\mathbf{r}(T)$ are almost independent, and the signal becomes simply the square of the form factor of the confining domain. For restricted diffusion between parallel planes at distance L, one gets

$$E \propto \frac{\sin^2(\gamma\delta g L/2)}{(\gamma\delta g L/2)^2} . \quad (5)$$

In this limit, a Gaussian-type behavior approximately manifests only when $\gamma\delta g L \ll 1$. Coy and Callaghan observed a considerable deviation from the GPA prediction in a PGSE experiment using a stack of pentane-filled microcapillaries.[32]

It should be noted, however, that the PGSE signal measured in the long-time limit is in fact independent of the diffusive motion. For instance, Eq. (5) does not contain the free-diffusion coefficient. This property is a specific feature of PGSE experiments and the related narrow-pulse approximation. In contrast, a temporal profile continuously encoding the whole spin trajectory (like Hahn's bipolar profile) was expected to yield the motional narrowing regime at long T [like Eq. (3)], that is, a Gaussian behavior. The restricted diffusion between parallel planes in the case of a steady temporal profile was studied by Stoller *et al.*, who predicted a failure of the g^2 behavior for intense magnetic fields.[33,34] Several years later, Hürlimann *et al.* observed a non-Gaussian attenuation of the signal in this so-called localization regime.[35] They measured the macroscopic signal of water molecules diffusing between two parallel plates of separation 0.16 mm and found spectacular deviation between the cases when the bipolar gradient was applied parallel to the plates (unrestricted diffusion, Gaussian regime) and perpendicular to the plates (restricted diffusion, localization regime). The remarkable result of this experiment was that the GPA broke down at ordinary gradient intensities as small as 15 mT/m.

A qualitative reason for the GPA breakdown is simple. Since the motion is restricted, infinitesimal increments of the accumulated phase φ are not independent, and φ is not necessarily a Gaussian variable. As a consequence, its second moment is no longer the only contribution determining the signal attenuation. When the diffusion-sensitizing magnetic fields are intense, the contribution of the higher order moments becomes dominant, and the GPA fails.

Although the qualitative picture was more or less clear, the transition between the GPA and the localization regime raised open questions. What are the limits of applicability of both regimes? Which kind of behavior should be expected in between? Since a non-Gaussian attenuation can be observed under ordinary experimental conditions, these questions are far from being purely of academic interest. In this light, it may appear striking how little we know about the high-order moments. So, Bergman and Dunn calculated the fourth moment in the case of a periodic porous medium.[36] A general representation for the high-order moments in terms of the Laplace operator eigenbasis was proposed in Refs. 13, 15, and 37. (see Sec. II). However, the computation of these moments in general still presented a challenge, even at numerical level.

In this paper, we solve this problem for restricted diffusion between parallel planes in a cosine magnetic field. The specific choice of the spatial profile as proportional to an eigenfunction of the Laplace operator in this confining geometry allowed us to considerably simplify the underlying mathematics. In particular, we found exact and explicit relations for the second and several higher order moments. These results helped us to study the general structure and the properties of the high-order moments, as well as a deviation from the GPA at magnetic fields of moderate or high intensity. From these observations, we could deduce quantitative estimates for the limits of applicability of the GPA in the case of a cosine magnetic field. Although this spatial profile is indeed very specific (e.g., its experimental realization presents a challenge in itself), the deduced properties of the high-order moments provide a better understanding of the GPA and its limitations in general. Moreover, our numerical simulations showed that the explicit relations obtained in the case of a cosine magnetic field can be used as good approximations for usually applied linear magnetic field gradients, for which the theoretical analysis was in general limited to the second moment. Note also that Zielinski and Sen considered the cosine spatial profile to model and study susceptibility-induced local magnetic fields.[38]

The paper is organized as follows. In the next section, we recall the basic theoretical relations to describe restricted diffusion in inhomogeneous magnetic fields. In Sec. III, we show how this general matrix formalism can be applied to study restricted diffusion between parallel planes in a cosine magnetic field. An iterative technique is proposed in Sec. IV to perform multiple integration in the computation of the time averages for a steady temporal profile. In Sec. V, we discuss the properties of the high-order moments, as well as a deviation from the GPA and transition between different restricted diffusion regimes.

II. MATRIX DESCRIPTION OF RESTRICTED DIFFUSION

In this section, we outline the theoretical description of restricted diffusion in inhomogeneous magnetic fields that originates from the work of Robertson,[26] who employed the Laplace operator eigenfunctions to tackle the Bloch-Torrey equation.[39] Since his work, a number of theoretical and numerical extensions have been suggested. So, Caprihan *et al.* introduced a multiple-narrow-pulse approximation to study restricted diffusion in a time-varying magnetic field gradient.[40] Callaghan proposed an elegant matrix formalism that could easily be implemented to perform efficient numerical computations.[41,42] An alternative approach was developed by Barzykin.[43,44] All these matrix formalisms focused on the case of a linear magnetic field gradient. A more general theoretical description for arbitrary spatial and temporal profiles was given by Axelrod and Sen[13] and later reformulated by Grebenkov[15,37] as the multiple correlation function (MCF) approach. In what follows, we recall the

basic theoretical relations of this approach that will then be applied to study restricted diffusion in a cosine magnetic field.

In a simple spin-echo experiment, the combination of the first 90° radio-frequency (rf) pulse at time $t=0$ and the second 180° rf pulse at time $T/2$ allows one to excite and to refocus the spin magnetizations in a way to form an echo at time T. Between these rf pulses, a time-dependent spatially inhomogeneous magnetic field $B_t(\mathbf{r})$ is superposed with a constant field B_0 to encode diffusive motion. Let us write $B_t(\mathbf{r})=\beta f(t)B(\mathbf{r})$, where $f(t)$ and $B(\mathbf{r})$ are the normalized temporal and spatial profiles of the magnetic field of intensity β, respectively. Note that the spin inversion by the 180° rf pulse is effectively represented via $f(t)$. The accumulated phase can be written as $\varphi=q\phi$, where

$$q=\gamma\beta T$$

is the dimensionless magnetic field strength[45] (e.g., $q=\gamma gTL$ for a linear gradient), while

$$\phi=\int_0^1 dt\, f(t)B(X_t), \tag{6}$$

is the normalized phase, X_t being the reflected Brownian motion confined in a bounded domain Ω with impenetrable (reflecting) boundary $\partial\Omega$. We shall use the dimensionless time t ranging from 0 to 1.

The macroscopic spin-echo signal is obtained by averaging the transverse spin magnetizations $e^{iq\phi}$ over the large ensemble of diffusing spins. As a consequence, the signal appears as the characteristic function of the random variable ϕ,

$$E=\mathbb{E}\{e^{iq\phi}\}, \tag{7}$$

where $\mathbb{E}$ denotes the expectation of the functional in parentheses over all stochastic trajectories X_t. The signal is normalized to have $E(q=0)=1$.

For unrestricted diffusion in a linear magnetic field gradient, ϕ is a Gaussian random variable, giving

$$E^{\mathrm{GPA}}=\exp(-q^2\mathbb{E}\{\phi^2/2\}), \tag{8}$$

in agreement with (1). For restricted diffusion, ϕ is a bounded variable, so that the signal E is an analytic function of q that can be expanded into absolutely converging series,

$$E=\sum_{n=0}^{\infty}(iq)^n\mathbb{E}\{\phi^n/n!\}. \tag{9}$$

The moments $\mathbb{E}\{\phi^n/n!\}$ depend on the following:

- the geometry of the confining domain Ω;
- the applied magnetic field [profiles $f(t)$ and $B(\mathbf{r})$];
- and the dimensionless diffusion coefficient $p=DT/L^2$ showing how fast the spins diffuse in the domain Ω of a characteristic size L.

To investigate these dependences, the moments $\mathbb{E}\{\phi^n/n!\}$ can be represented by means of two infinite-dimension matrices $\mathcal{B}$ and Λ,

$$\mathcal{B}_{m,m'}=\int_\Omega d\mathbf{r}\; u_m^*(\mathbf{r})B(\mathbf{r})u_{m'}(\mathbf{r}), \tag{10}$$

$$\Lambda_{m,m'}=\delta_{m,m'}\lambda_m, \tag{11}$$

where λ_m and $u_m(\mathbf{r})$ are the normalized eigenvalues and eigenfunctions of the Laplace operator Δ in the confining domain Ω,

$$-\Delta u_m(\mathbf{r})=\frac{\lambda_m}{L^2}u_m(\mathbf{r})\quad(\mathbf{r}\in\Omega), \tag{12}$$

$$\frac{\partial u_m}{\partial n}=0\quad(\mathbf{r}\in\partial\Omega). \tag{13}$$

The Neumann (or reflecting) boundary condition (13) describes the frontier $\partial\Omega$ with no surface relaxation.[46] In this case, the moments were found to be[13,15,37]

$$\mathbb{E}\left\{\frac{\phi}{n!}\right\}=\left\langle\left[\mathcal{B}e^{-p(t_2-t_1)\Lambda}\mathcal{B}\cdots\mathcal{B}e^{-p(t_n-t_{n-1})\Lambda}\mathcal{B}\right]_{0,0}\right\rangle_n, \tag{14}$$

where the subscript 0,0 denotes the first diagonal element of the matrix product in square brackets. The (ordered) f-weighted time average $\langle\ldots\rangle_n$ was defined for any function $F(t_1,\ldots,t_n)$ of n variables $t_1,\ldots,t_n$ as multiple integral

$$\langle F(t_1,\ldots,t_n)\rangle_n=\int_0^1 dt_1\, f(t_1)\ldots\int_{t_{n-1}}^1 dt_n\, f(t_n)F(t_1,\ldots,t_n). \tag{15}$$

For example,

$$\langle(t_2-t_1)\rangle_2=\int_0^1 dt_1\, f(t_1)\int_{t_1}^1 dt_2\, f(t_2)(t_2-t_1).$$

The leading asymptotic behavior of the even-order moments in the slow diffusion regime ($p\ll 1$) was argued to be[15]

$$\mathbb{E}\{\phi^{2n}/(2n)!\}\simeq p^n\frac{(\langle(t_1-t_2)\rangle_2)^n}{n!}\left(\frac{L^{2n}}{V}\int_\Omega d\mathbf{r}|\nabla B(\mathbf{r})|^{2n}\right)+O(p^{n+1/2}), \tag{16}$$

V being the volume of the confining domain Ω. In the motional narrowing regime ($p\gg 1$), one expected

$$\mathbb{E}\{\phi^{2n}/(2n)!\}\simeq p^{-n}\frac{\zeta_{-1}^n}{n!}\left(\int_0^1 dt\, f^2(t)\right)^n+O(p^{-n-1}), \tag{17}$$

where the coefficients ζ_ℓ were defined for $\ell\leq 1$ as

$$\zeta_\ell=\sum_{m=1}^{\infty}\mathcal{B}_{0,m}\lambda_m^\ell\mathcal{B}_{m,0}. \tag{18}$$

The calculation of the high-order moments $\mathbb{E}\{\phi^n/n!\}$ is in general a very difficult task. While the second moment was already investigated in detail in Neuman's work,[27] very few authors have dealt with the fourth moment.[36] The difficulty is evident: multiplication of the infinite-dimension matrices $\mathcal{B}$ and Λ in (14) leads to a huge combination of exponential functions $e^{-p\lambda_k(t_{k+1}-t_k)}$ that should then be averaged

with the effective temporal profile $f(t)$ according to the multiple integration in (15). In general, this problem is intractable even numerically.

III. COSINE MAGNETIC FIELD

In this section, we show how the choice of the cosine magnetic field in a slab geometry simplifies the structure of the matrix $\mathcal{B}$. More precisely, we consider restricted diffusion between parallel planes at distance 1, which is equivalent to diffusion on the interval $(0,1)$ with reflections at the endpoints $x=0$ and $x=1$. The Laplace operator eigenbasis is well known,

$$\lambda_m = \pi^2 m^2, \quad u_m(x) = \varepsilon_m \cos(\pi m x), \tag{19}$$

where $\varepsilon_m = \sqrt{2}$ for $m>0$, and $\varepsilon_0 = 1$, to ensure the normalization

$$\int_0^1 dx\, u_m(x) u_n^*(x) = \delta_{m,n}.$$

We consider the magnetic field of the cosine spatial profile

$$B(x) = \cos(\pi \kappa x), \tag{20}$$

where κ is a fixed strictly positive integer. A direct calculation gives

$$\frac{1}{V}\int_\Omega d\mathbf{r} |\nabla B(\mathbf{r})|^{2n} = (\pi\kappa)^{2n} \frac{\Gamma(n+1/2)}{\sqrt{\pi}\Gamma(n+1)}, \tag{21}$$

which determines the slow diffusion asymptotic behavior (16) of the moments $\mathbb{E}\{\phi^n/n!\}$ [here $\Gamma(z)$ is the Euler function].

Choosing the magnetic field (20) to be proportional to an eigenfunction of the Laplace operator yields a simple structure of the matrix $\mathcal{B}$,

$$\mathcal{B}_{m,m'} = \frac{\varepsilon_m \varepsilon_{m'}}{4}(\delta_{m',m+\kappa} + \delta_{m',m-\kappa} + \delta_{m',-m+\kappa}), \tag{22}$$

where the fourth Kronecker symbol $\delta_{m',-m-\kappa}$ is omitted since m and m' are positive integers, while κ is a strictly positive integer.

Let us first consider the case $\kappa=1$, when the matrix $\mathcal{B}$ consists of two subdiagonals,

$$\mathcal{B} = \begin{pmatrix} 0 & \sqrt{2}/2 & 0 & 0 & 0 & \cdots \\ \sqrt{2}/2 & 0 & 1/2 & 0 & 0 & \cdots \\ 0 & 1/2 & 0 & 1/2 & 0 & \cdots \\ 0 & 0 & 1/2 & 0 & 1/2 & \cdots \\ 0 & 0 & 0 & 1/2 & 0 & \cdots \\ \cdots & \cdots & \cdots & \cdots & \cdots & \cdots \end{pmatrix}.$$

This structure can be written analytically as

$$\mathcal{B}_{m,m'} = \frac{1}{\varepsilon_m \varepsilon_{m'}}(\delta_{m',m+1} + \delta_{m',m-1}). \tag{23}$$

In particular, the substitution of the above relation into the definition (18) yields $\zeta_\ell = \lambda_1^\ell/2$. According to (17), the coefficient $\zeta_{-1} = (2\lambda_1)^{-1}$ determines the asymptotic behavior of the moments $\mathbb{E}\{\phi^n/n!\}$ in the motional narrowing regime $(p \gg 1)$.

The substitution of (23) into the matrix product in (14) gives

$$\mathbb{E}\{\varphi^n/n!\} = \left\langle \sum_{m_1,\ldots,m_{n-1}=0}^{\infty} \left(\frac{\delta_{0,m_1\pm1}}{\varepsilon_0\varepsilon_{m_1}}\right) e^{-p(t_2-t_1)\lambda_{m_1}} \times \left(\frac{\delta_{m_1,m_2\pm1}}{\varepsilon_{m_1}\varepsilon_{m_2}}\right) e^{-p(t_3-t_2)\lambda_{m_2}} \ldots e^{-p(t_n-t_{n-1})\lambda_{m_{n-1}}} \times \left(\frac{\delta_{m_{n-1},0\pm1}}{\varepsilon_{m_{n-1}}\varepsilon_0}\right) \right\rangle_n, \tag{24}$$

where we formally write $\delta_{m',m\pm1}$ instead of the sum $\delta_{m',m+1} + \delta_{m',m-1}$. The first and the last Kronecker symbols imply $m_1 = m_{n-1} = 1$. Nontrivial contributions come only from such sequences of indices $m_1,\ldots,m_{n-1}$ for which $m_{i+1} - m_i = \pm 1$. Consequently, the sequence $m_1,\ldots,m_{n-1}$ can be thought of as successive positions of a random walker on the one-dimensional lattice.[47] This walk starts at site 1 and is conditioned to return to the same site after $n-2$ steps. Since the indices m_i should be positive, this walk is reflected at site 0. As a result, the sum over all positive indices $m_1,\ldots,m_{n-1}$ with the above Kronecker symbols can be replaced by a sum over all reflected trajectories $m_1 \to \ldots \to m_{n-1}$ of length $n-2$ from 1 to 1,

$$\mathbb{E}\{\phi^n/n!\} = \left\langle \sum_{m_1\to\ldots\to m_{n-1}} \frac{1}{\varepsilon_0 \varepsilon_{m_1}^2 \ldots \varepsilon_{m_{n-1}}^2 \varepsilon_0} \times \exp[-p\lambda_{m_1}(t_2-t_1) \ldots - p\lambda_{m_{n-1}}(t_n - t_{n-1})] \right\rangle_n.$$

Using the definitions of the coefficients ε_m and the eigenvalues λ_m, one gets

$$\mathbb{E}\{\phi^n/n!\} = \sum_{m_1\to\ldots\to m_{n-1}} 2^{-N(m_1,\ldots,m_{n-1})} \times \left\langle \exp\left[-p\lambda_1 \sum_{i=1}^{n-1} m_i^2 (t_{i+1} - t_i)\right] \right\rangle_n,$$

where $N(m_1 \ldots m_{n-1})$ is the number of positions m_j such that $m_j \neq 0$. As shown in Appendix A, the general case with $\kappa > 1$ can be treated in the same way simply by replacing λ_1 with λ_κ:

$$\mathbb{E}\{\phi^n/n!\} = \sum_{m_1\to\ldots\to m_{n-1}} 2^{-N(m_1,\ldots,m_{n-1})} \times \left\langle \exp\left[-p\lambda_\kappa \sum_{i=1}^{n-1} m_i^2 (t_{i+1} - t_i)\right] \right\rangle_n. \tag{25}$$

A direct analogy between the moments of the accumulated phase and random walks will help us to deduce a number of results. For instance, the condition of returning to the starting position $(m_1 = m_{n-1} = 1)$ immediately implies that the trajectory length $n-2$ must be even. This simple argument shows that all odd moments $\mathbb{E}\{\phi^{2n+1}\}$ vanish for any temporal profile $f(t)$.

To better illustrate this analogy, let us now consider several even moments. In the simplest case $n=2$, there is a single "trajectory" $m_1=1$ of length 0 leading to

$$\mathbb{E}\{\phi^2/2\} = \frac{1}{2}\langle \exp[-p\lambda_\kappa(t_2-t_1)]\rangle_2. \tag{26}$$

This is exact result for the cosine magnetic field. For $n=4$, there are two trajectories of length 2,

$$\begin{array}{ccccccc} m_1 & & m_2 & & m_3 & & 2^{-N} \\ 1 & \rightarrow & 0 & \rightarrow & 1 & & (1/2)^2, \\ 1 & \rightarrow & 2 & \rightarrow & 1 & & (1/2)^3 \end{array}$$

giving

$$\mathbb{E}\{\phi^4/4!\} = \frac{1}{4}\langle \exp[-p\lambda_\kappa(1^2(t_2-t_1)+1^2(t_4-t_3))]\rangle_4 + \frac{1}{8}\langle \exp[-p\lambda_\kappa(1^2(t_2-t_1)+2^2(t_3-t_2) + 1^2(t_4-t_3))]\rangle_4.$$

In the case $n=6$, there are five trajectories of length 4,

$$\begin{array}{ccccccccccc} m_1 & & m_2 & & m_3 & & m_4 & & m_5 & & 2^{-N} \\ 1 & \rightarrow & 0 & \rightarrow & 1 & \rightarrow & 0 & \rightarrow & 1 & & (1/2)^3 \\ 1 & \rightarrow & 2 & \rightarrow & 1 & \rightarrow & 0 & \rightarrow & 1 & & (1/2)^4 \\ 1 & \rightarrow & 0 & \rightarrow & 1 & \rightarrow & 2 & \rightarrow & 1 & & (1/2)^4 \\ 1 & \rightarrow & 2 & \rightarrow & 1 & \rightarrow & 2 & \rightarrow & 1 & & (1/2)^5 \\ 1 & \rightarrow & 2 & \rightarrow & 3 & \rightarrow & 2 & \rightarrow & 1 & & (1/2)^5 \end{array}.$$

In a similar way, one can consider higher order moments. The computation becomes more and more time-consuming since the number of trajectories grows rapidly with n. For instance, the eighth, tenth, and twelfth moments would require 14, 42, and 132 trajectories, respectively. Nonetheless, the specific choice of the cosine spatial profile allowed us to reduce the difficult matrix manipulations of the spatial averages to a simple combinatorial relation (25). The analogy with one-dimensional random walks made its practical implementation for numerical or symbolic computation easier (see below). The problem of the temporal averaging $\langle \ldots \rangle_n$ is addressed in the next section.

IV. ANALYSIS OF TEMPORAL AVERAGES

In order to find explicit formulas for the moments $\mathbb{E}\{\phi^n/n!\}$, one needs to calculate the f-weighted time average,

$$\langle \exp[-p\lambda_\kappa(m_1^2(t_2-t_1)+\cdots+m_{n-1}^2(t_n-t_{n-1}))]\rangle_n,$$

as a function of p with fixed indices $m_1,\ldots,m_{n-1}$. This quantity was defined in (15) as a multiple integral with a given effective temporal profile $f(t)$ of the magnetic field. In other words, we should deal with integrals of generic form

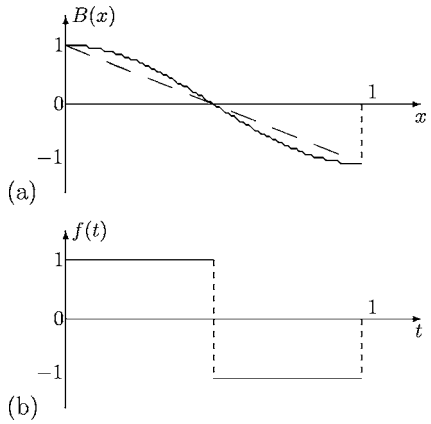

FIG. 1. Spatial (a) and temporal (b) profiles of the magnetic field used in this paper. A linear gradient profile is shown on (a) for comparison. Note the sign change of the temporal profile $f(t)$ at $t=1/2$ accounting for the 180° rf pulse.

$$I_n(\alpha_1,\ldots\alpha_n) = \int_0^1 dt_1\, f(t_1)e^{\alpha_1 t_1}\int_{t_1}^1 dt_2\, f(t_2)e^{\alpha_2 t_2}\cdots \times \int_{t_{n-2}}^1 dt_{n-1}\, f(t_{n-1})e^{\alpha_{n-1}t_{n-1}}\int_{t_{n-1}}^1 dt_n\, f(t_n)e^{\alpha_n t_n}, \tag{27}$$

where

$$\alpha_j = \begin{cases} p\lambda_\kappa m_1^2 & (j=1) \\ p\lambda_\kappa(m_j^2-m_{j-1}^2) & (j=2,\ldots,n-1) \\ -p\lambda_\kappa m_{n-1}^2 & (j=n) \end{cases}. \tag{28}$$

For an arbitrary function $f(t)$, the simplest numerical technique to compute this expression would be a Monte Carlo integration. In fact, the multiple integral can be thought of as an "expectation" of the integrand function. To approximate $I_n(\alpha_1,\ldots,\alpha_n)$, one repeatedly evaluates the integrand function for randomly chosen moments $0\le t_1\le\ldots\le t_n\le 1$, and then takes the average value over a large number of trials. This technique can be easily implemented for any temporal profile,[48] and the computational time increases linearly with the moment order n.

An analytical computation of the multiple integral (27) is much more difficult. In what follows, we consider two particular choices of the function $f(t)$: a Stejskal-Tanner profile with two very narrow rectangular pulses, and a steady profile shown in Fig. 1(b).

A. Narrow-pulse approximation

In the short or narrow-pulse approximation, when the effective temporal profile $f(t)$ consists of two very narrow pulses of duration $\delta\ll 1$ at moments $t=0$ and $t=1/2$, a number of theoretical results can be deduced. In particular, we obtain the approximation of the f-weighted time average of a function $F(t_1,\ldots,t_n)$ by the sum

$$\langle F(t_1,\ldots,t_n)\rangle_n \simeq \frac{\delta^n}{n!}\sum_{k=0}^{n}(-1)^k C_n^k F\left(0,0,\ldots,\underbrace{\frac{1}{2},\frac{1}{2}}_{k\text{ times}}\right),$$

where C_n^k are the binomial coefficients. For instance,

$$\langle F(t_1,t_2)\rangle_2 \simeq \frac{\delta^2}{2}\left(F(0,0)-2F\left(0,\frac{1}{2}\right)+F\left(\frac{1}{2},\frac{1}{2}\right)\right).$$

Taking

$$F(t_1,\ldots,t_n)=\prod_{j=1}^{n}e^{\alpha_j t_j},$$

one can reduce the computation of the multiple integral (27) to combinatorial analysis. It is still a challenging problem since the f-weighted time averages then have to be summed over different sets of indices α_j according to Eq. (25).

There is however a simpler way to obtain the moments $\mathbb{E}\{\phi^n/n!\}$ within the narrow-pulse approximation. As shown in Appendix B, one can directly use the specific properties of the cosine spatial profile of the magnetic field to get

$$\mathbb{E}\{\phi^{2n}/(2n)!\} \simeq \delta^{2n}\frac{(2n)!}{2^{2n}(n!)^2}\sum_{m=0}^{n}\frac{(-1)^m\varepsilon_m^2 e^{-p\lambda_m/2}}{(n-m)!\,(n+m)!}. \quad (29)$$

We shall come back to this expression in Sec. V C.

B. Steady profile

For a steady magnetic field, the effective temporal profile shown in Fig. 1(b) satisfies two simple properties,

$$f^2(t)=1,\quad f(1-t)=-f(t).$$

We are looking for the multiple integral in (27) that can be seen as a successive application of a kind of integration operator. If the operator $\mathcal{A}_\alpha$ with index α acts on a function $g(t)$ as

$$[\mathcal{A}_\alpha g](t)=\int_t^1 dt'\, e^{\alpha t'}f(t')g(t'), \quad (30)$$

then the f-weighted time average can be written as

$$I_n(\alpha_1,\ldots,\alpha_n)=[\mathcal{A}_{\alpha_1}\mathcal{A}_{\alpha_2}\ldots\mathcal{A}_{\alpha_n}1]\ \ (t=0). \quad (31)$$

The successive application of these operators can be treated iteratively. First, a direct integration shows that the application of the operator $\mathcal{A}_{\alpha_n}$ with $\alpha_n\neq 0$ to the constant 1 or to the function $f(t)$ is a linear combination of 1 and $f(t)$, whose coefficients contain an exponential function $e^{\alpha_n t}$,

$$[\mathcal{A}_{\alpha_n}1](t)=\frac{e^{\alpha_n/2}-e^{\alpha_n}}{\alpha_n}+\frac{e^{\alpha_n/2}-e^{\alpha_n t}}{\alpha_n}f(t),$$

$$[\mathcal{A}_{\alpha_n}f](t)=\frac{e^{\alpha_n}-e^{\alpha_n t}}{\alpha_n}. \quad (32)$$

The exponential function $e^{\alpha_n t}$ only "shifts" [cf. definition (30)] the index of the next operator $\mathcal{A}_{\alpha_{n-1}}$ that will be applied to this linear combination afterward. As a consequence, the further application of the operators $\mathcal{A}_{\alpha_{n-1}}$, $\mathcal{A}_{\alpha_{n-2}}$,... would always be expressed through a linear combination of 1 and $f(t)$ with different exponential functions, if their indices (and "shifted" indices) were always nonzero. In our analysis however, this condition cannot be satisfied. When at some moment $\alpha=0$, the application of the operator $\mathcal{A}_0$ to 1 or $f(t)$ leads to a linear combination involving "new" functions t and $tf(t)$. The general case is considered in Appendix C: if $g(t)$ is a linear combination of monomials t^k with coefficients which may contain exponential functions and $f(t)$, then $[\mathcal{A}_\alpha g](t)$ is a linear combination of the same kind. Moreover, if n is the maximum degree of monomials in $g(t)$, then $[\mathcal{A}_\alpha g](t)$ has the same maximum degree n when $\alpha\neq 0$, and the degree $n+1$ for $\alpha=0$. This property allows one to represent the action of the operator $\mathcal{A}_\alpha$ to a given combination $g(t)$ of monomials as a linear transformation of its coefficients. As a consequence, the computation of the multiple integral in (31) can be reduced to a product of finite-dimension matrices.

This technique can be used for both analytical and numerical calculation of the f-weighted time average. In the former case, the matrix representation can be implemented in software supporting symbolic analysis like, e.g., MATLAB, MAPLE, or MATHEMATICA. The result would be an explicit dependence of $I_n(\alpha_1,\ldots,\alpha_n)$ on the parameters $\alpha_1,\ldots,\alpha_n$. As an example, let us derive the f-weighted time average for the second moment. In this case, $\alpha_1=p\lambda_\kappa$ and $\alpha_2=-p\lambda_\kappa$. Using $\alpha_1=-\alpha_2=\alpha$, one finds

$$[\mathcal{A}_\alpha\mathcal{A}_{-\alpha}1](t)=\frac{e^{-\alpha/2}-2+\alpha}{\alpha^2}+\frac{e^{-\alpha/2}-1}{\alpha^2}f(t)$$
$$-\frac{e^{-\alpha}-e^{-\alpha/2}}{\alpha^2}e^{\alpha t}f(t)+\frac{e^{-\alpha/2}}{\alpha^2}e^{\alpha t}-\frac{1}{\alpha}t.$$

Taking $t=0$ according to Eq. (31), one gets

$$I_2(\alpha,-\alpha)=\frac{1}{\alpha^2}(\alpha-3+4e^{-\alpha/2}-e^{-\alpha}), \quad (33)$$

so that

$$\langle\exp[-p\lambda_m(t_2-t_1)]\rangle_2=I_2(p\lambda_m,-p\lambda_m).$$

The structure of the above expression can already be recognized in Neuman's work.[27] According to (26), the second moment for the cosine magnetic field is

$$\mathbb{E}\{\phi^2/2\}=\frac{1}{2}\left(\frac{1}{p\lambda_\kappa}-\frac{e^{-p\lambda_\kappa}-4e^{-p\lambda_\kappa/2}+3}{p^2\lambda_\kappa^2}\right). \quad (34)$$

We stress again that this is an exact dependence of the second moment on the dimensionless diffusion coefficient p.

In a similar way, one can derive explicit and exact formulas for the higher order moments,

$$\mathbb{E}\{\phi^4/4!\}=\frac{1}{1152\tilde{p}^4}(144\tilde{p}^2-1116\tilde{p}+2943-96\tilde{p}e^{-\tilde{p}/2}+4336e^{-\tilde{p}/2}+240\tilde{p}e^{-\tilde{p}}+1392e^{-\tilde{p}}+16e^{-2\tilde{p}}$$
$$-16e^{-5\tilde{p}/2}+e^{-4\tilde{p}}), \tag{35}$$

$$\mathbb{E}\{\phi^6/6!\}=\frac{1}{4\ 147\ 200\tilde{p}^6}$$
$$\times\begin{pmatrix}86\ 400\tilde{p}^3-1\ 231\ 200\tilde{p}^2+7\ 493\ 400\tilde{p}-18\ 769\ 800\\+(7200\tilde{p}^2-642\ 000\tilde{p}+28\ 929\ 300)e^{-\tilde{p}/2}-(180\ 000\tilde{p}^2+2\ 545\ 800\tilde{p}+10\ 159\ 775)e^{-\tilde{p}}\\+(13\ 440\tilde{p}-53\ 376)e^{-2\tilde{p}}+(12\ 960\tilde{p}+53\ 896)e^{-5\tilde{p}/2}\\-(120\tilde{p}+248)e^{-4\tilde{p}}+76e^{-9\tilde{p}/2}-96e^{-5\tilde{p}}+24e^{-13\tilde{p}/2}-e^{-9\tilde{p}}\end{pmatrix}, \tag{36}$$

where $\tilde{p}=p\lambda_\kappa$. As one would expect, the number of terms grows rapidly with the order n. The expression for the eighth moment used to plot Figs. 3 and 4 is not present.

V. DISCUSSION

In this section, we discuss the physical meaning of the above mathematical results.

A. The second moment

Before proceeding with the analysis of the high order moments, it is worth glancing at $\mathbb{E}\{\phi^2/2\}$ as the dominant contribution to the macroscopic spin-echo signal at magnetic fields of small intensity ($q\ll 1$). The choice of the cosine magnetic field led us to a simple form (34) of the second moment for a steady temporal profile. An important feature of this relation is that $\mathbb{E}\{\phi^2/2\}$ is an analytic function of the dimensionless diffusion coefficient p. This situation is different with respect to the classical case of a linear magnetic field gradient. In fact, the general expression for the second moment is

$$\mathbb{E}\{\phi^2/2\}=\sum_{m=0}^{\infty}\mathcal{B}_{0,m}I_2(p\lambda_m,-p\lambda_m)\mathcal{B}_{m,0},$$

where I_2 is given by (33). For the cosine magnetic field, $\mathcal{B}_{0,m}=\mathcal{B}_{m,0}=2^{-1/2}\delta_{m,\kappa}$, the only term with $m=\kappa$ "survives" in the above sum. In general however, the sum contains an infinite number of terms. The rate of decrease of the matrix elements $\mathcal{B}_{0,m}$ as $m\to\infty$ determines the asymptotic behavior of the second moment as $p\ll 1$ (see Ref. 15). This problem was first studied by Mitra *et al.* for a linear gradient[3,16,17] and further extended by Axelrod and Sen[13] as

$$\mathbb{E}\{\phi^2/2\}\simeq\langle(t_1-t_2)\rangle_2\zeta_1 p+\langle(t_2-t_1)^{3/2}\rangle_2\zeta_{3/2}p^{3/2}+O(p^2), \tag{37}$$

where the time averages account for the effective temporal profile $f(t)$, while the spatial inhomogeneity of the magnetic field is represented by two coefficients ζ_1 and $\zeta_{3/2}$,[49]

$$\zeta_1=\frac{L^2}{V}\int_\Omega d\mathbf{r}|\nabla B(\mathbf{r})|^2, \tag{38}$$

$$\zeta_{3/2}=\frac{4}{3\sqrt{\pi}}\frac{L^3}{V}\int_{\partial\Omega}d\mathbf{r}\left(\frac{\partial B}{\partial n}\right)^2. \tag{39}$$

One can see that the nonanalytic $p^{3/2}$ dependence of the second moment is related to the properties of the magnetic field near the boundary. In the case of a linear magnetic field gradient in a slab, a cylinder, and a sphere, $\zeta_{3/2}$ is not zero. In contrast, the first derivative of the cosine magnetic field vanishes at the boundary, $B'(x)=-\pi\kappa\sin(\pi\kappa x)=0$ at $x=0$ and $x=1$, so that $\zeta_{3/2}=0$.

Apart from the above discrepancy, the second moments for the cosine magnetic field and linear gradient are quite similar. In particular, one can use the simple explicit relation (34) with $\kappa=1$ to approximate the second moment in the case of a linear gradient,

$$\mathbb{E}\{\phi^2/2\}^{\cos}=\frac{\pi^2}{120}\left(\frac{1}{p\pi^2}-\frac{e^{-p\pi^2}-4e^{-p\pi^2/2}+3}{p^2\pi^4}\right). \tag{40}$$

The additional prefactor $\pi^2/60$ effectively accounts for the difference between two spatial profiles in the motional nar-

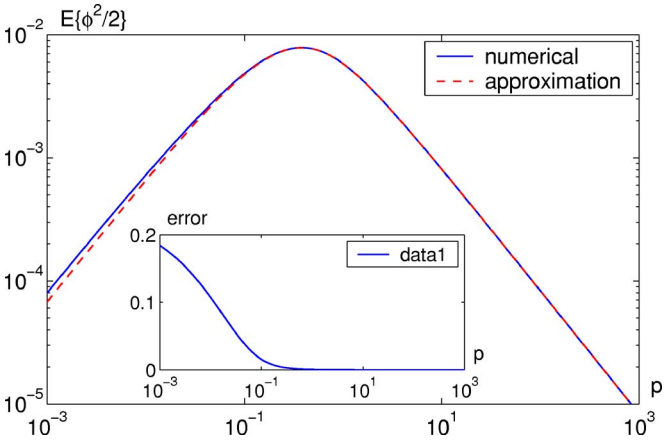

FIG. 2. Numerically computed second moment $\mathbb{E}\{\phi^2/2\}^{\text{lin}}$ for a linear gradient as a function of p and its approximation (40). The inset shows relative deviation between them.

rowing regime. In fact, this is the ratio between the coefficient ζ_{-1} for a linear gradient ($\zeta_{-1}=1/120$) and for the cosine magnetic field ($\zeta_{-1}=1/2\pi^2$).

In Fig. 2, we compare the relation (40) and the numerically computed second moment $\mathbb{E}\{\phi^2/2\}^{\text{lin}}$ for a linear magnetic field gradient.[50] The inset of Fig. 2 shows a relative deviation between these quantities as a function of p. In the slow diffusion regime, this deviation can be estimated as $1-\pi^4/120\simeq 0.1883$ by comparing the series expansion of Eq. (40) and the leading term $p/12$ of $\mathbb{E}\{\phi^2/2\}^{\text{lin}}$ as $p\to 0$. As expected, the subtle information about the slow diffusion limit is lost within this approximation. Surprisingly, the maximum of the second moment as a function of p for both spatial profiles appears at nearly the same value of the dimensionless diffusion coefficient p_m. From Eq. (40), one finds numerically $p_m\simeq 0.3836$.

One may also wonder whether the oscillating character of the cosine magnetic field is relevant or not. To answer this question, we considered in Appendix D the sine magnetic field, $B(x)=\sin \pi\kappa x$. Since the only difference between the sine and cosine functions is a phase shift, one could expect to obtain similar results. On the contrary, we found quite different behavior in both the slow diffusion and the motional narrowing regimes. We conclude that the properties of the cosine magnetic field result from the fact that its spatial profile is proportional to an eigenfunction of the Laplace operator in a slab geometry, as well as from its first derivative vanishing at the boundary.

B. Higher order moments

We can now proceed with the analysis of the higher order moments. Using explicit forms of the fourth, sixth, and eighth moments [Eqs. (35) and (36)], we first check the asymptotic relations (16) and (17) in the slow diffusion and the motional narrowing regimes. For a steady temporal profile, one can substitute the averages

$$\langle (t_1-t_2)\rangle_2=\frac{1}{12}\quad \int_0^1 dt\, f^2(t)=1,$$

into Eqs. (16) and (17) to get

$$\mathbb{E}\{\phi^{2n}/(2n)!\}\simeq p^n\left(\frac{\pi^2\kappa^2}{12}\right)^n\frac{\Gamma(n+1/2)}{\sqrt{\pi}(n!)^2}+O(p^{n+1/2}),$$

$$\mathbb{E}\{\phi^{2n}/(2n)!\}\simeq p^{-n}\frac{1}{2(\pi^2\kappa^2)^n n!}+O(p^{-n-1}),$$

for $p\to 0$ and $p\to\infty$, respectively. The comparison with explicit relations [like Eq. (35) for the fourth moment] confirms the above asymptotic results.

Figure 3 shows the second, fourth, sixth, and eighth moments as functions of p. As expected, higher order moments have much smaller amplitudes. However, the contribution of each moment $\mathbb{E}\{\phi^{2n}/(2n)!\}$ is weighted by q^{2n} in the series expansion (9). If the dimensionless magnetic field strength q is big enough, the high-order moments may contribute much more than the second moment. In this case, the GPA would not be valid anymore.

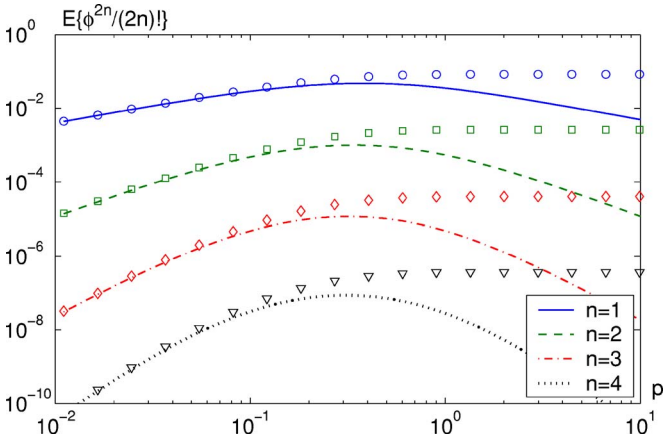

FIG. 3. Second, fourth, sixth, and eighth moments as functions of p for the cosine magnetic field ($\kappa=1$). For comparison, the NPA predictions (43) are shown by empty symbols (see Sec. V C).

To estimate the limits of its applicability, one can expand the Gaussian form (8) into a series

$$E^{\text{GPA}}=\sum_{n=0}^{\infty}(-q^2)^n\frac{(\mathbb{E}\{\phi^2/2\})^n}{n!}.$$

Since the odd moments vanish for the cosine spatial profile, the exact series expansion (9) can be rewritten as

$$E=\sum_{n=0}^{\infty}(-q^2)^n\mathbb{E}\{\phi^{2n}/(2n)!\}.$$

The comparison of these expansions term by term leads to a Gaussian approximation for the high-order moments,

$$\mathbb{E}\{\phi^{2n}/(2n)!\}^{\text{GPA}}\equiv\frac{(\mathbb{E}\{\phi^2/2\})^n}{n!}. \tag{41}$$

The ratios $\mathcal{E}_n(p)$ between the moments and their Gaussian approximations are shown in Fig. 4 for $n=1,2,3,4$. As expected, this function goes to 1 as $p\to\infty$ according to the asymptotic relation (17). In the opposite limit $p\to 0$, one finds

$$\mathcal{E}_n(0)=\frac{\Gamma(n+1/2)}{\sqrt{\pi}\Gamma(n+1)}.$$

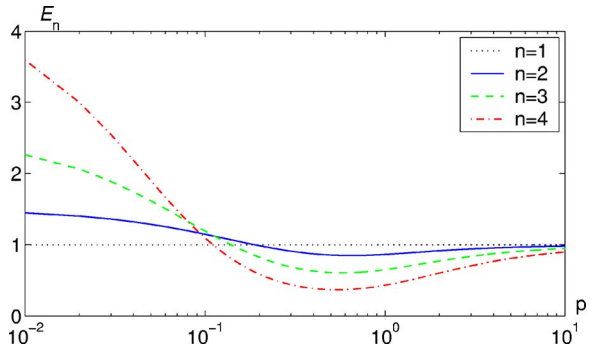

FIG. 4. Ratio between the moments $\mathbb{E}\{\phi^{2n}/(2n)!\}$ for the cosine magnetic field ($\kappa=1$) and their Gaussian approximations $(\mathbb{E}\{\phi^2/2\})^n/n!$ for $n=1,2,3,4$.

When the GPA is valid, the deviations between the high-order moments and their Gaussian approximations are small. More precisely, this condition can be written for $n>1$ as

$$q^{2n}|\mathbb{E}\{\phi^{2n}/(2n)!\} - \mathbb{E}\{\phi^{2n}/(2n)!\}^{\mathrm{GPA}}| \ll q^2\mathbb{E}\{\phi^2/2\},$$

or, equivalently, as

$$q \ll q_n(p) = \sqrt{\frac{1}{\mathbb{E}\{\phi^2/2\}}\frac{(n!)^{1/(n-1)}}{|\mathcal{E}_n(p)-1|^{1/(n-1)}}}. \tag{42}$$

To estimate the limits of applicability of the GPA,[51] we check this condition for $n=2$. The asymptotic behavior of $q_2(p)$ as $p\to 0$ and $p\to\infty$ is $(96/\lambda_\kappa)^{1/2}/\sqrt{p}$ and $(16\lambda_\kappa^2/7)^{1/2}p$, respectively. If $\kappa=1$, one gets two simple estimates for the slow diffusion and the motional narrowing regimes: $q\ll 3/\sqrt{p}$ and $q\ll 15p$, respectively. For intermediate values of p, one numerically finds the minimum of $q_2(p)$, giving $q\ll 4.15$. We shall return to these estimates in Sec. V F.

At this point, we should outline an important difference between linear and nonlinear spatial profiles of the magnetic field. The asymptotic form (16) of the moments $\mathbb{E}\{\phi^{2n}/(2n)!\}$ in the slow diffusion regime contains the integral of the magnetic field gradient $\nabla B(\mathbf{r})$ in power $2n$ over the confining domain Ω. When $B(\mathbf{r})$ is a linear function of the spatial coordinates, its gradient is constant, $L^2|\nabla B(\mathbf{r})|^2=1$, and one has for any n

$$\frac{L^{2n}}{V}\int_\Omega d\mathbf{r}|\nabla B(\mathbf{r})|^{2n} = 1.$$

As a consequence, the Gaussian approximation (41) holds in the slow diffusion limit, since $\mathcal{E}_n(0)=1$. In this case, $\mathcal{E}_n(p)$ would deviate from 1 only for intermediate values of p. For nonlinear spatial profiles (like cosine or parabolic magnetic fields), this is not true, and $\mathcal{E}_n(p)$ deviates from 1 for intermediate and small p as shown in Fig. 4. As a result, the Gaussian phase approximation should in general work "better" for a linear gradient than for a nonlinear magnetic field.

C. Comparison with NPA

The narrow-pulse approximation has been widely used to study the signal attenuation by restricted diffusion. In particular, it allowed us to obtain the explicit form (29) of the moments $\mathbb{E}\{\phi^{2n}/(2n)!\}$ for arbitrary n. It is now worth comparing this simple relation to that of the high-order moments in the case of a steady temporal profile. For this purpose, one has to renormalize Eq. (29) in an appropriate way. In fact, although the diffusing spins are "exposed" at the magnetic field of the same intensity q, the duration of this field differs for the narrow-pulse and steady temporal profiles. In other words, the effective attenuation of the signal is different. To renormalize the explicit relation (29), one can look at the asymptotic form (16) in the slow diffusion regime. The f-weighted averages $\langle(t_1-t_2)\rangle_2$ for the narrow-pulse and steady temporal profiles are equal to $\delta^2/2$ and $1/12$, respectively. As a consequence, one has to multiply Eq. (29) by $(1/12)^n/(\delta^2/2)^n$, giving

$$\mathbb{E}\{\phi^{2n}/(2n)!\}^{\mathrm{NPA}} \simeq \frac{(2n)!}{24^n(n!)^2}\sum_{m=0}^{n}\frac{(-1)^m\varepsilon_m^2 e^{-p\lambda_m/2}}{(n-m)!\,(n+m)!}. \tag{43}$$

A very simple structure of this relation might be employed for theoretical studies of the high-order moments. Figure 3 helps to compare the NPA-based prediction (43) with the exact relations for a steady temporal profile. Although one could find a good agreement in the slow diffusion regime ($p\to 0$), drastic deviations appear when p goes to infinity. In fact, the exponential functions in (43) vanish rapidly as $p\to\infty$, leading to a constant asymptotic limit of the effective moments,

$$\lim_{p\to\infty}\mathbb{E}\{\phi^{2n}/(2n)!\}^{\mathrm{NPA}} = \frac{(2n)!}{24^n(n!)^4}.$$

This behavior evidently contradicts the asymptotic relation (17) in the motional narrowing regime. In this light, the GPA-based relation (41) appears to be more convenient to represent the general structure of the high-order moments. We conclude that, in spite of an apparent efficiency of the NPA for theoretical analysis, this approximation may lead to unrealistic results when the magnetic field pulses are not narrow enough. The limits of applicability of the NPA have been thoroughly discussed in the literature (Ref. 15 and references therein).

D. Series expansion of the moments

Since the moment $\mathbb{E}\{\phi^{2n}/(2n)!\}$ is an analytic function of p in the case of a cosine magnetic field, it can be expanded into a power series,

$$\mathbb{E}\{\phi^{2n}/(2n)!\} = \sum_{j=0}^{\infty}(-1)^{n-j}c_{2n,j}(p\lambda_\kappa)^j, \tag{44}$$

where the dependence on λ_κ is written explicitly for convenience as well as the factor $(-1)^{n-j}$. Expanding the exponential function in (25), one can deduce the expression for the coefficients $c_{2n,j}$,

$$c_{2n,j} = \frac{(-1)^n}{j!}\sum_{m_1\to\cdots\to m_{2n-1}} 2^{-N(m_1\cdots m_{2n-1})} \times\left\langle\left[\sum_{i=1}^{2n-1}(t_{i+1}-t_i)m_i^2\right]^j\right\rangle_{2n}. \tag{45}$$

The asymptotic relation (16) implies that $c_{2n,j}=0$ for $j<n$, and

$$c_{2n,n} = \left(\frac{1}{12}\right)^n\frac{\Gamma(n+1/2)}{\sqrt{\pi}(n!)^2}.$$

Moreover, the simple expression (34) for the second moment gives for $n=1$

$$c_{2,j} = \frac{1}{2}\frac{1-2^{-j}}{(j+2)!}.$$

The computation of $c_{2n,j}$ for $n>1$ (and $j>n$) can be performed numerically according to (45).

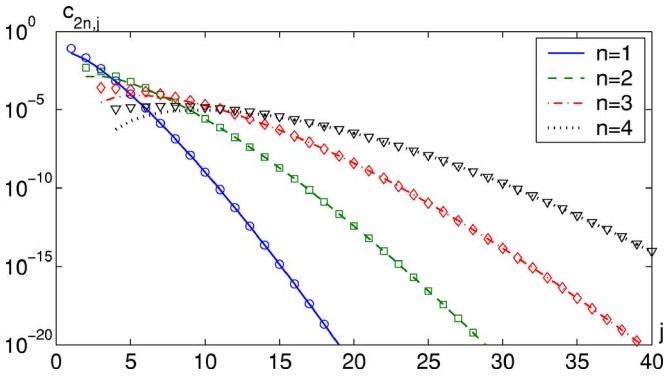

FIG. 5. Coefficients $c_{2n,j}$ and their asymptotic approximations $\tilde{c}_{2n,j}$ (shown by empty symbols) as functions of j for $n=1,2,3,4$.

At theoretical level, one can obtain the leading asymptotic terms $\tilde{c}_{2n,j}$ of the coefficients $c_{2n,j}$ as $j\to\infty$. For this purpose, let us consider Eq. (35) for the fourth moment and expand the exponential functions in power series. For large value of j, the leading term $\tilde{p}^j$ is dominated by the expansion of $e^{-4\tilde{p}}$, from which the following asymptotic approximation can be derived:

$$\tilde{c}_{4,j}=\frac{1}{1152}\frac{4^{j+4}}{(j+4)!}.$$

In the general case, the main contribution to $c_{2n,j}$ as $j\to\infty$ is provided by $e^{-n^2\tilde{p}}$. Its series expansion up to the order j gives

$$\tilde{c}_{2n,j}=\frac{2^{3-2n}}{[(2n)!]^2}\frac{(n^2)^{j+2n}}{(j+2n)!}, \tag{46}$$

where the first numerical prefactor came from the combinatorial coefficient in front of $e^{-n^2\tilde{p}}$.

The coefficients $c_{2n,j}$ as functions of j and their asymptotic approximations $\tilde{c}_{2n,j}$ are plotted for several n values in Fig. 5. One can see an excellent agreement between them when $j>2n$. While $c_{2,j}$ monotonously decreases with j, the other coefficients $c_{2n,j}$ as functions of j show nonmonotonic behavior. As a result, the lowest order asymptotic approximation (16) of the high-order moments would be valid only for very small p. When p increases, higher order corrections in p become significant.

E. Localization regime

When the dimensionless magnetic field strength q is big enough, the contribution of the high-order moments becomes dominant, and the GPA is not valid anymore. In principle, the absolutely converging series expansion (9) might still be used to calculate the signal attenuation. However, when q is large, one needs a greater number of terms to ensure accurate computation. This point can be illustrated with a simple example. The exponential function e^{-x} can always be computed by its series expansion. However, even for $x=2$, one needs at least eight terms to get the result with an accuracy on the order of 1%. The difference between e^{-x} and the signal E is that the coefficients of the series expansion (9) are the moments $\mathbb{E}\{\phi^{2n}/(2n)!\}$. Even in the case of the steady cosine magnetic field, their computation is difficult and time-consuming for large values of n. For this reason, a perturbative approach becomes useless in practice for large q.

A nonperturbative approach to study the localization regime was first developed by Stoller *et al.* for a linear magnetic field gradient in a slab geometry.[33] They showed that the Bloch-Torrey equation[39] for the magnetization could be reduced to the Airy equation, and the asymptotic signal attenuation was found to be

$$E\propto\exp\left[-(a_1/2)(pq^2)^{1/3}\right], \tag{47}$$

where $a_1\simeq 1.0188$ was the absolute value of the first zero of the derivative of the Airy function.[52] This behavior was argued to be valid for other confining geometries by de Swiet and Sen,[34] while Hürlimann *et al.* gave its experimental confirmation.[35]

In the literature, the localization regime is often considered as a "pathological" or "anomalous" situation, in comparison with the classical and widely used Gaussian phase approximation. It should be noted, however, that as soon as diffusive motion is geometrically restricted, the GPA does break down for relatively intense magnetic fields. In other words, the localization regime is an *intrinsic* feature of restricted diffusion.

The localization regime for the cosine magnetic field (with $\kappa=1$) was investigated by Zielinski and Sen.[38] In this case, the Bloch-Torrey equation can be reduced to the Mathieu equation, from which the following asymptotic behavior was deduced for $q\gg 1$:

$$E\propto\exp\left[-(\pi/2)(pq)^{1/2}\right]. \tag{48}$$

Both relations (47) and (48) state that the signal exhibits a non-Gaussian stretch-exponential attenuation. The related exponent depends on the magnetic field spatial profile: 2/3 for a linear gradient and 1/2 for the cosine magnetic field. The dependence on p is also different.

To illustrate the transition between the GPA and the localization regime, the macroscopic spin-echo signal was computed numerically for the cosine magnetic field by means of the MCF approach.[15,37] The dependence of this signal on q is plotted in Fig. 6 for several values of p. At small values of q, one observes the Gaussian behavior. This is a simple consequence of the first-order approximation in the series expansion (9),

$$E\simeq 1-q^2\mathbb{E}\{\phi^2/2\}+O(q^4)\simeq\exp(-q^2\mathbb{E}\{\phi^2/2\})+O(q^4).$$

When p is small, the second moment can be approximated by its leading term proportional to p in the slow diffusion regime [Fig. 6(a)]. When p increases, the Gaussian behavior can still be observed for small q, but the second moment is now proportional to $1/p$ (the motional narrowing regime), as shown in Figs. 6(b) and 6(c). In the case $p=10$, the deviation between the GPA prediction and the numerically computed signal becomes significant only for $q\geq 40$.

When q increases, a transition to a non-Gaussian regime is observed for all three plots. The location of the transition region on the q axis depends on the dimensionless diffusion coefficient p: for smaller p, smaller q is needed for breakdown of the GPA. As shown in Fig. 6, the signal attenuation at the localization regime follows the stretch-exponential law

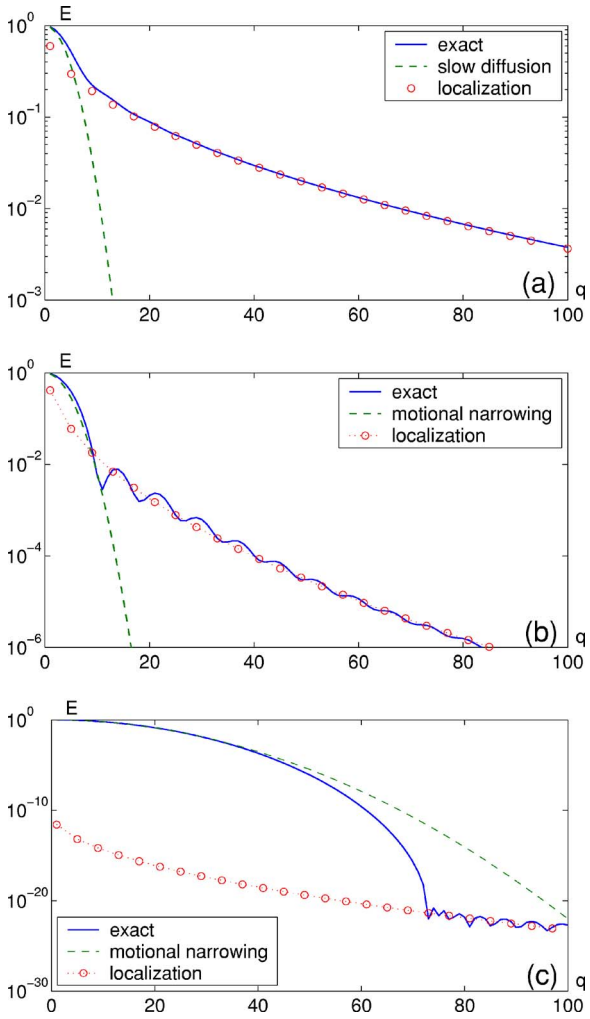

FIG. 6. Breakdown of the GPA in the case of the cosine magnetic field ($\kappa=1$) for three values of the dimensionless diffusion coefficient: $p=0.1$ (a), $p=1$ (b), and $p=10$ (c). Similar trend can be found for a linear magnetic field gradient (not shown).

(48) derived by Zielinski and Sen.[53] However, some kind of oscillatory behavior can be seen for the curves at $p=1$ and $p=10$ (similar trends were observed in Refs. 54 and 55).

F. Transition between different regimes

From the mathematical point of view, the breakdown of the GPA always takes place for large enough values of q. It may however happen that the transition between the GPA and the localization regime occurs when the signal is negligible, as illustrated by Fig. 6(c). This means that the localization regime cannot be observed in such experimental conditions. In this situation, the GPA would correctly describe experimental measurements.

A complete pq diagram of different restricted diffusion regimes is depicted in Fig. 7(a). The signal is attenuated by a factor of 2 at each line separating two adjacent gray-scale regions (appearing as pale and dark stripes). The first large pale region on the left is composed of points (q,p) for which the signal E lies between 1/2 and 1. The next dark stripe regroups points (q,p) for which $1/4 \leq E \leq 1/2$, and so on. The white area on the right corresponds to pairs (q,p) for which the signal is below 10^{-3}. Since such a small signal is often comparable to noise, this area is referred to as "inaccessible experimentally." In this pq diagram, the bold line delimits the region on the left in which the GPA predictions of the signal attenuation are valid with an accuracy of at least 5%. The thin and dashed lines show the limits of the slow diffusion and the motional narrowing regimes, in which Eqs. (16) and (17) give results with an accuracy of at least 5%. Note that the bold line is somewhat similar to the estimate $q_2(p)$ but it is naturally "shifted" to the left (smaller q) with respect to $q_2(p)$.

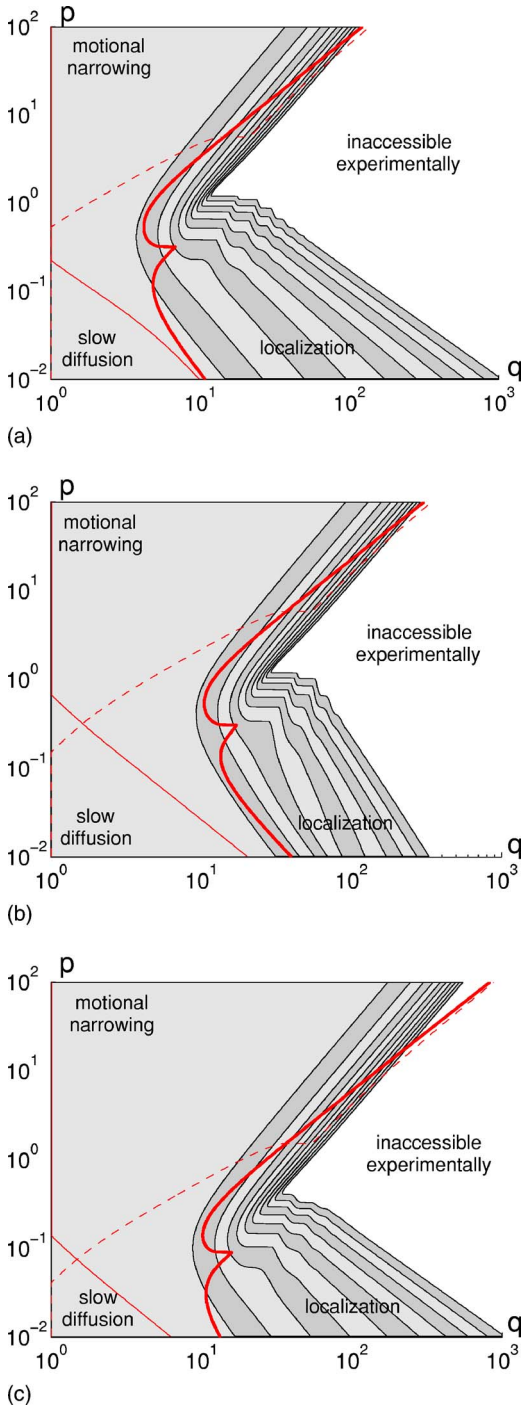

FIG. 7. Transition between different regimes of restricted diffusion for the cosine magnetic field with $\kappa=1$ (a, top), a linear gradient (b, middle), and the sine magnetic field with $\kappa=1$ (c, bottom). See the text for description.

For the whole region on the right of the bold line, the Gaussian phase approximation fails to predict accurate results. Apart from the transient region in the vicinity of this line, the localization regime is expected for larger q values. However, if p is not small enough, the signal attenuation is too strong for large values of q, driving us to the area which is "inaccessible experimentally." Conversely, the localization regime can be experimentally observed for relatively small p. For instance, Hürlimann's experiment[35] with water molecules was realized with p on the order of 0.01.

It is worth noting that the GPA in the slow diffusion regime (small p) is valid for weakly attenuated signals only (the first pale region). In contrast, the GPA in the motional narrowing regime describes the signal attenuation in a much wider range. Surprisingly, the GPA based on the first (leading)-order approximation (17) seems to better approximate the signal attenuation for large q than that for the precisely computed second moment (in Fig. 7, the dashed line intersects the bold line and goes in a deeper region to the right). This "anomalous" behavior is caused by the contribution of the higher order moments that become significant for large q values.

For comparison, the pq diagram for the case of a linear gradient and the sine magnetic field are plotted in Figs. 7(b) and 7(c), respectively. Their structure is very similar to that of Fig. 7(a). One can note that the stripes are thinner for small values of p and "shifted" to the right (to larger values of q) for a linear gradient. In turn, the diagram for the sine magnetic field is "shifted" to the bottom (to smaller values of p). Such diagrams can be used in practice to estimate the signal for given parameters p and q. From this plot, one can also determine which kind of restricted diffusion is expected, and which formula should be applied to fit experimental data. Note, however, that this information is rather qualitative since the particular location of different regions on the diagram depends on the confining geometry.

VI. CONCLUSION

Apart from the narrow-pulse approximation, the main attention in theoretical analysis of diffusive NMR phenomena has been focused for a long time on the second moment of the total accumulated phase. On one hand, this moment provided the major contribution to the macroscopic spin-echo signal at magnetic fields with relatively small inhomogeneity found in typical experimental conditions. On the other hand, the computation of the higher order moments presented a very difficult problem, even at numerical level. To tackle this problem theoretically, the high-order moments were expressed in terms of the Laplace operator eigenbasis so that the spatial magnetic field profile and the confining geometry were represented in (14) via two infinite-dimension matrices $\mathcal{B}$ and Λ, while the effective temporal profile $f(t)$ was taken into account as the f-weighted time average.[13,15,37] The matrix product and the multiple integration in (14) are in general difficult to calculate for the fourth and higher order moments. To overcome this problem, we considered restricted diffusion between parallel planes in a cosine magnetic field which was proportional to an eigenfunction of the Laplace operator in this confining geometry. This choice led us to a much simpler structure of the matrix $\mathcal{B}$ than for other spatial profiles. In particular, we were able to reduce the computation of the high-order moments to the analysis of lattice random walks in one dimension. An iterative technique was then proposed to calculate the f-weighted time averages in the case of a steady temporal profile. For the first time, exact and explicit dependences of several moments on the dimensionless diffusion coefficient p were obtained.

The properties of these moments were investigated in detail. We have shown that these moments are analytic functions of p. For instance, the second moment did not exhibit the classical $p^{3/2}$ behavior in the slow diffusion regime. This is a specific feature of the cosine magnetic field as its first derivative vanishes at the boundary. Conversely, the general structures of the second moment are very similar for the cosine magnetic field and linear gradient. In particular, the explicit relation (40) provides a good approximation for the second moment in the case of a linear gradient (except for small p). This approximation appeared to be more accurate than theoretical predictions based on the NPA. In this light, the consideration of "odd" spatial profiles such as a cosine magnetic field is justified as a very efficient "toy" model allowing derivation of analytical results that can be used further as approximations for more realistic magnetic fields.

A deviation of the fourth and higher order moments from their Gaussian form (41) was then investigated and shown to be important for small and intermediate values of p. This deviation is responsible for the breakdown of the Gaussian phase approximation, when the dimensionless magnetic field strength q is large enough. We also outlined a significant difference between linear and nonlinear spatial profiles of the magnetic field in the slow diffusion regime. In fact, the Gaussian form (41) is not valid for nonlinear magnetic fields as $p \to 0$.

Finally, we plotted the pq diagram where different regimes of restricted diffusion were shown together. In the same figure, we provided gray-scale zebra representation of the signal attenuation to outline which regime would be accessible experimentally. In particular, predictions in the motional narrowing regime ($p \gg 1$) were shown to be valid even for strongly attenuated signals. On the other hand, the increase of the magnetic field strength q in the slow diffusion limit ($p \ll 1$) led to the localization regime. As a consequence, the GPA appeared to work "better" for larger values of p. Further investigation would help to better understand the transition between the Gaussian and localization regimes. Although very specific, the cosine magnetic field appears to be a promising choice of the spatial profile to simplify the underlying mathematics of restricted diffusion in NMR.

APPENDIX A: EXTENSION TO $\kappa > 1$

The general case $\kappa > 1$ can be considered in exactly the same way as $\kappa = 1$. So, the matrix $\mathcal{B}$ is written as

$$\mathcal{B}_{m,m'} = \frac{1}{\varepsilon_m \varepsilon_{m'}} \left(\delta_{m,m'-\kappa} + \delta_{m,m'+\kappa} + \sum_{j=1}^{\kappa-1} \delta_{m,j} \delta_{m',\kappa-j} \right). \tag{A1}$$

For instance, one has for $\kappa=2$

$$\mathcal{B} = \begin{pmatrix} 0 & 0 & \sqrt{2}/2 & 0 & 0 & \cdots \\ 0 & 1/2 & 0 & 1/2 & 0 & \cdots \\ \sqrt{2}/2 & 0 & 0 & 0 & 1/2 & \cdots \\ 0 & 1/2 & 0 & 0 & 0 & \cdots \\ 0 & 0 & 1/2 & 0 & 0 & \cdots \\ \cdots & \cdots & \cdots & \cdots & \cdots & \cdots \end{pmatrix}.$$

In general, the computation of multiple products of such matrices would lead to cumbersome expressions. A crucial simplification comes from the fact that we are interested only in the first diagonal element of these products. If m is a multiple of κ, m' should be a multiple of κ too. To illustrate this point, an analogy with lattice random walks may be useful. Starting from $m=0$, the walker necessarily jumps to $m_1=\kappa$. Then, it can choose between $m_2=0$ and $m_2=2\kappa$, and so on. Since the intermediate sites (which are not multiples of κ) cannot be "visited," the third term in (A1) does not influence the computation of the moments, and thus can be omitted. In other words, the moments $\mathbb{E}\{\phi^n/n!\}$ can be *exactly* computed with a simplified matrix $\tilde{\mathcal{B}}$,

$$\tilde{\mathcal{B}}_{m,m'} = \frac{1}{\varepsilon_m \varepsilon_{m'}} (\delta_{m,m'-\kappa} + \delta_{m,m'+\kappa}). \tag{A2}$$

As a consequence, one can directly use the results derived in Sec. III for $\kappa=1$, with the only substitution of λ_1 by λ_κ.

APPENDIX B: ANALYSIS BY NARROW-PULSE APPROXIMATION

In the narrow-pulse approximation, the accumulated phase in (6) can be approximately written as

$$\phi \simeq \delta B(X_0) - \delta B(X_{1/2}),$$

where X_0 and $X_{1/2}$ are random positions of a spin at times $t=0$ and $t=1/2$ when the narrow diffusion-sensitizing pulses were applied. For a uniform initial distribution of spins, the signal simply becomes

$$E = \frac{1}{V} \int_\Omega d\mathbf{r}_0 \int_\Omega d\mathbf{r}\; e^{iq\delta(B(\mathbf{r}_0)-B(\mathbf{r}))} G_{1/2}(\mathbf{r}_0,\mathbf{r}),$$

where the Green function $G_{1/2}(\mathbf{r}_0,\mathbf{r})$ is the probability density for a spin starting from $\mathbf{r}_0$ at time $t=0$ to arrive in the vicinity of $\mathbf{r}$ at time $t=1/2$. Expanding the exponential function in a power series, one finds the even moments within the NPA,

$$\mathbb{E}\{\phi^{2n}/(2n)!\} = \frac{\delta^{2n}}{(2n)!} \times \int_\Omega d\mathbf{r}_1 \int_\Omega d\mathbf{r}_2\; G_{1/2}(\mathbf{r}_1,\mathbf{r}_2)(B(\mathbf{r}_1) - B(\mathbf{r}_2))^{2n}.$$

This double integral can be explicitly found for restricted diffusion between parallel planes in a cosine magnetic field. In this case, the spectral decomposition of the Green function leads to

$$\mathbb{E}\{\phi^{2n}/(2n)!\} = \frac{\delta^{2n}}{(2n)!} \sum_{m=0}^{\infty} \varepsilon_m^2 e^{-p\lambda_m/2} \int_0^1 dx_1 \int_0^1 dx_2\; \cos(\pi m x_1) \times \cos(\pi m x_2)(\cos(\pi x_1) - \cos(\pi x_2))^{2n} \tag{B1}$$

(here we used $\kappa=1$ for the sake of simplicity). The binomial expansion of the expression in the big parentheses and further combinatorial simplifications yield

$$\int_0^1 dx_1 \int_0^1 dx_2\; \cos(\pi m x_1)\cos(\pi m x_2)(\cos(\pi x_1) - \cos(\pi x_2))^{2n} = \left(\frac{(2n)!}{2^n n!} \right)^2 \frac{(-1)^m}{(n-m)!\,(n+m)!}.$$

Since this integral is equal to 0 for $m>n$, the sum in (B1) is truncated to the upper limit $m=n$, and one retrieves Eq. (29).

APPENDIX C: PROPERTIES OF THE OPERATOR $\mathcal{A}_\alpha$

To calculate the average (31), we consider how the operator $\mathcal{A}_\alpha$ acts on exponential and polynomial functions.

- Exponential functions: From the definition (30), one gets the following relation for any function $g(t)$:

$$[\mathcal{A}_\alpha e^{\alpha' t} g](t) = [\mathcal{A}_{\alpha+\alpha'} g](t), \tag{C1}$$

  i.e., the exponential function $e^{\alpha' t}$ "shifts" the index α to $\alpha+\alpha'$.

- Polynomials: A direct calculation shows that

$$[\mathcal{A}_\alpha t^n] = (-1)^n \frac{n!}{\alpha^{n+1}} \left[\left(e^{\alpha/2} \sum_{k=0}^{n} \frac{(-\alpha/2)^k}{k!} - e^{\alpha} \sum_{k=0}^{n} \frac{(-\alpha)^k}{k!} \right) + \left(e^{\alpha/2} \sum_{k=0}^{n} \frac{(-\alpha/2)^k}{k!} \right) f(t) - e^{\alpha t} \sum_{k=0}^{n} \frac{(-\alpha)^k}{k!} t^k f(t) \right], \tag{C2}$$

  for $\alpha \neq 0$, and

$$[\mathcal{A}_0 t^n] = \frac{(1/2)^{n+1} - 1}{n+1} + \frac{(1/2)^{n+1}}{n+1} f(t) - \frac{1}{n+1} t^{n+1} f(t). \tag{C3}$$

- Polynomials with $f(t)$: In a similar way, one finds

$$[\mathcal{A}_\alpha t^n f] = (-1)^n \frac{n!}{\alpha^{n+1}} \left(e^{\alpha} \sum_{k=0}^{n} \frac{(-\alpha)^k}{k!} - e^{\alpha t} \sum_{k=0}^{n} \frac{(-\alpha)^k}{k!} t^k \right), \tag{C4}$$

  for $\alpha \neq 0$, and

$$[\mathcal{A}_0 t^n f] = \frac{1}{n+1} - \frac{1}{n+1} t^{n+1}. \tag{C5}$$

It is easy to show that the computation of the moment of order $2n$ requires monomials t^k of the maximum degree n. In

other words, a successive application of the operators $\mathcal{A}_{\alpha_1},\ldots,\mathcal{A}_{\alpha_n}$, from the right to the left in (31), gives a linear combination of monomials t^k $(k\leq n)$ with coefficients which may contain exponential functions and $f(t)$. One may thus think of a "linear space" spanned over a set of these functions. Using the above relations, one constructs the matrices representing the action of the operators $\mathcal{A}_{\alpha_1},\ldots,\mathcal{A}_{\alpha_n}$ in this space. The computation of the f-weighted time average (27) is then reduced to a product of finite-dimension matrices.

APPENDIX D: SINE MAGNETIC FIELD

Unlike linear magnetic field gradient, the cosine profile is an oscillating function. One may thus wonder whether this particular property is relevant or not. To answer this question, we consider the sine spatial profile $B(x)=\sin\pi\kappa x$. Since the only difference between the sine and cosine functions is a phase shift, one could expect to obtain similar results. In particular, one finds the identical leading terms in the slow diffusion limit since

$$\frac{1}{V}\int_\Omega d\mathbf{r}|\nabla B|^2=\frac{\pi^2\kappa^2}{2}.$$

As one will see below, this is the only apparent similarity between these spatial profiles.

For the sine magnetic field, the elements $\mathcal{B}_{m,m'}$ are

$$\mathcal{B}_{m,m'}=\frac{\varepsilon_m\varepsilon_{m'}\kappa}{\pi}\frac{(1-(-1)^{\kappa+m+m'})(\kappa^2-m^2-m'^2)}{(\kappa^2-m^2-m'^2)^2-4m^2m'^2}.$$

The asymptotic behavior of the second moment in the motional narrowing regime is determined by coefficient ζ_{-1}. According to the definition (18), one writes

$$\zeta_\ell=2\kappa^2\pi^{2\ell-2}\sum_{m=1}^{\infty}\frac{(1-(-1)^{\kappa+m})^2m^{2\ell}}{(\kappa^2-m^2)^2}.$$

The Laplace transform technique described in Ref. 15 can be used to calculate these coefficients analytically. In particular, one finds

$$\zeta_{-1}=\begin{cases}\dfrac{5\pi^2\kappa^2-48}{6\pi^4\kappa^4} & (\text{odd }\kappa)\\ \dfrac{3}{2\pi^2\kappa^2} & (\text{even }\kappa)\end{cases},$$

$$\zeta_{-2}=\begin{cases}\dfrac{\pi^4\kappa^4+210\pi^2\kappa^2-2160}{180\pi^6\kappa^6} & (\text{odd }\kappa)\\ \dfrac{\pi^2\kappa^2+30}{12\pi^4\kappa^4} & (\text{even }\kappa)\end{cases}.$$

These relations give much smaller coefficients ζ_{-1} and ζ_{-2} in comparison to their counterparts $\zeta_\ell=(\pi\kappa)^{2\ell}/2$ for the cosine magnetic field. This leads to a slower signal attenuation in the motional narrowing regime.

The distinction between these two spatial profiles is significant even in the slow diffusion limit. While the leading terms are identical, their first corrections are different. For the cosine magnetic field, one deduces from (34)

$$\mathbb{E}\{\phi^2/2\}=\frac{\pi^2\kappa^2}{24}p-\frac{\pi^4\kappa^4}{64}p^2+O(p^3).$$

In the case of the sine spatial profile, one finds

$$\mathbb{E}\{\phi^2/2\}=\frac{\pi^2\kappa^2}{24}p-\frac{8\pi^2\kappa^2}{3\sqrt{\pi}}\frac{4-\sqrt{2}}{35}p^{3/2}+O(p^2).$$

This nonanalytical behavior of the second moment is similar to (37) for a linear gradient suggested by Mitra *et al.*

[1] P. T. Callaghan, *Principles of Nuclear Magnetic Resonance Microscopy* (Clarendon, Oxford, 1991).
[2] P. T. Callaghan, A. Coy, D. MacGowan, K. J. Packer, and F. O. Zelaya, Nature **351**, 467 (1991).
[3] P. P. Mitra, P. N. Sen, L. M. Schwartz, and P. Le Doussal, Phys. Rev. Lett. **68**, 3555 (1992).
[4] W. P. Halperin, J.-Y. Jehng, and Y.-Q. Song, Magn. Reson. Imaging **12**, 169 (1994).
[5] M. D. Hürlimann, K. G. Helmer, L. L. Latour, and C. H. Sotak, J. Magn. Reson., Ser. A **111**, 169 (1994).
[6] M. D. King, J. Houseman, S. A. Roussel, N. van Bruggen, S. R. Williams, and D. G. Gadian, Magn. Reson. Med. **32**, 707 (1994).
[7] R. W. Mair, G. P. Wong, D. Hoffmann, M. D. Hürlimann, S. Patz, L. M. Schwartz, and R. L. Walsworth, Phys. Rev. Lett. **83**, 3324 (1999).
[8] Y.-Q. Song, S. Ryu, and P. N. Sen, Nature **406**, 178 (2000).
[9] V. G. Kiselev and D. S. Novikov, Phys. Rev. Lett. **89**, 278101 (2002).
[10] H. E. Möller, X. J. Chen, B. Saam, K. D. Hagspiel, G. A. Johnson, T. A. Altes, E. E. de Lange, and H.-U. Kauczor, Magn. Reson. Med. **47**, 1029 (2002).
[11] E. J. R. van Beek, J. M. Wild, H.-U. Kauczor, W. Schreiber, J. P. Mugler III, and E. E. de Lange, J. Magn. Reson Imaging **20**, 540 (2004).
[12] D. Le Bihan, Nat. Rev. Neurosci. **4**, 469 (2003).
[13] S. Axelrod and P. N. Sen, J. Chem. Phys. **114**, 6878 (2001).
[14] P. N. Sen, Concepts Magn. Reson. **23A**, 1 (2004).
[15] D. S. Grebenkov, Rev. Mod. Phys. (2007) (in press).
[16] P. P. Mitra, P. N. Sen, and L. M. Schwartz, Phys. Rev. B **47**, 8565 (1993).
[17] L. L. Latour, P. P. Mitra, R. L. Kleinberg, and C. H. Sotak, J. Magn. Reson., Ser. A **101**, 342 (1993).
[18] K. G. Helmer, M. D. Hürlimann, T. M. de Swiet, P. N. Sen, and C. H. Sotak, J. Magn. Reson., Ser. A **115**, 257 (1995).
[19] B. T. Saam, D. A. Yablonskiy, V. D. Kodibagkar, J. C. Leawoods, D. S. Gierada, J. D. Cooper, S. S. Lefrak, and M. S. Conradi, Magn. Reson. Med. **44**, 174 (2000).
[20] D. A. Yablonskiy, A. L. Sukstanskii, J. C. Leawoods, D. S. Gierada, G. L. Bretthorst, S. S. Lefrak, J. D. Cooper, and M. S. Conradi, Proc. Natl. Acad. Sci. U.S.A. **99**, 3111 (2002).
[21] E. L. Hahn, Phys. Rev. **80**, 580 (1950).
[22] H. Y. Carr and E. M. Purcell, Phys. Rev. **94**, 630 (1954).
[23] D. E. Woessner, J. Chem. Phys. **34**, 2057 (1961).
[24] D. E. Woessner, J. Phys. Chem. **67**, 1365 (1963).
[25] E. O. Stejskal and J. E. Tanner, J. Chem. Phys. **42**, 288 (1965).
[26] B. Robertson, Phys. Rev. **151**, 273 (1966).
[27] C. H. Neuman, J. Chem. Phys. **60**, 4508 (1974).
[28] J. Stepišnik, Physica B & C **104**, 350 (1981).
[29] J. Stepišnik, Prog. Nucl. Magn. Reson. Spectrosc. **17**, 187 (1985).
[30] J. C. Tarczon and W. P. Halperin, Phys. Rev. B **32**, 2798 (1985).
[31] J. E. Tanner and E. O. Stejskal, J. Chem. Phys. **49**, 1768 (1968).
[32] A. Coy and P. T. Callaghan, J. Chem. Phys. **101**, 4599 (1994).
[33] S. D. Stoller, W. Happer, and F. J. Dyson, Phys. Rev. A **44**, 7459 (1991).
[34] T. M. de Swiet and P. N. Sen, J. Chem. Phys. **100**, 5597 (1994).
[35] M. D. Hürlimann, K. G. Helmer, T. M. de Swiet, P. N. Sen, and C. H. Sotak, J. Magn. Reson., Ser. A **113**, 260 (1995).
[36] D. J. Bergman and K.-J. Dunn, Phys. Rev. E **52**, 6516 (1995).
[37] D. S. Grebenkov, in Proceedings of the 8th International Bologna Conference on Magnetic Resonance in Porous Media, p. 54 (Bologna, Italy, 2006).
[38] L. J. Zielinski and P. N. Sen, J. Magn. Reson. **147**, 95 (2000).
[39] H. C. Torrey, Phys. Rev. **104**, 563 (1956).
[40] A. Caprihan, L. Z. Wang, and E. Fukushima, J. Magn. Reson., Ser. A **118**, 94 (1996).
[41] P. T. Callaghan, J. Magn. Reson. **129**, 74 (1997).

[42] S. L. Codd and P. T. Callaghan, J. Magn. Reson. **137**, 358 (1999).
[43] A. V. Barzykin, Phys. Rev. B **58**, 14171 (1998).
[44] A. V. Barzykin, J. Magn. Reson. **139**, 342 (1999).
[45] This dimensionless parameter q can be thought of as an extension of the classical q value in a PGSE experiment, $(2\pi)^{-1}\gamma g\delta$, to nonlinear and non-narrow magnetic fields.
[46] A more general Fourier (or mixed, or relaxing) boundary condition was considered in Ref. 15.
[47] We stress that this random walk is merely a useful analogy to manipulate the Kronecker symbols in (24). It has no relation to the physical diffusion of spins in a slab geometry.
[48] The efficiency and accuracy of this computation will, of course, depend on the temporal profile $f(t)$. For instance, if the content of $f(t)$ is too narrow (as in the case of Stejskal-Tanner narrow pulses), one needs to use specific distributions of moments $t_1,\ldots,t_n$ to perform trials.
[49] The integral representation (38) for ζ_1 can be rigorously derived from its definition (18). In contrast, this definition is in general not applicable to ζ_ℓ with $\ell>1$. The coefficient $\zeta_{3/2}$ is formally defined by series expansion (37) of the second moment as $p\to 0$; see Ref. 15 for details.
[50] The numerical implementation of the MCF approach to compute the signal attenuation in a linear magnetic field gradient was thoroughly discussed in Ref. 15. In this particular case, the MCF numerical technique is similar to the stepwise gradient approximation by Barzykin (Refs. 43 and 44).
[51] Although difficult to demonstrate rigorously, it is natural to assume that the next significant contribution after the second moment would be given by the fourth moment $(n=2)$.
[52] We stress again that this non-analytic dependence of the signal on q should be understood as asymptotic behavior.
[53] To better fit the signal as a function of q, we slightly modified the relation (48) by introducing an adjustable coefficient a_0, $E\propto\exp[-a_0(\pi/2)\times(pq)^{1/2}]$. We took a_0 equal to 1.13, 1.00, and 0.60 for $p=0.1$, $p=1$, and $p=10$, respectively. This minor modification may be related to some p-dependent corrections to the asymptotic behavior (48).
[54] A. L. Sukstanskii and D. A. Yablonskiy, J. Magn. Reson. **157**, 92 (2002).
[55] D. S. Grebenkov, J. Magn. Reson. **179**, 393 (2006).